Front instabilities in a forced oscillatory medium with global coupling

D. Battogtokh[1,2]
[1]*Center for Computational Physics, Department of Physics and Astronomy, The University of Georgia, Athens, Georgia 30602*
[2]*Physics and Technology Institute, Mongolian Academy of Sciences, Ulaanbaatar 51, Mongolia*
(Received 2 October 2002; published 6 December 2002)

We study a two-dimensional, locally and globally coupled oscillatory system that is subjected to external forcing at a frequency equal to twice its natural frequency. It is shown that the onset of an Ising-Bloch transition is preceded by novel front instabilities: a pattern formation instability, wave trains along the front, and a weak turbulence in the frontal patterns.

DOI: 10.1103/PhysRevE.66.066202 PACS number(s): 47.54.+r

I. INTRODUCTION

Bistable systems represent an important class in the theory of reaction and diffusion [1,2]. A front, sometimes called a kink, which connects the two stable states of bistability rules dynamics in such systems. A front is subject to different types of instabilities, depending on the nature of the system. For example, when a motionless front loses stability and starts propagation, it is called an Ising-Bloch transition. This type of instability has been observed in chemical reactions [3], and in liquid crystals [4].

Another type of front instability in dimension two has been studied by Kuramoto [5]. In this case, a front line, which initially represents a straight line, may undergo a long wave instability. It was shown that the resulting spatiotemporal chaotic dynamics of such a front can be described by the Kuramoto-Shivashinsky(KS) equation [6].

A convenient model for theoretical studies of front instabilities is externally forced coupled oscillators, where bistability arises from the broken rotational symmetry of the system. It was shown that depending on the intensity of the external forcing an Ising-Bloch transition occurs [7–9] in locally coupled oscillators.

In theoretical models as well as in experimental systems, local coupling, i.e., diffusional coupling, is not only the possible type of coupling between the oscillators. For example, in surface catalytic reactions both local and global couplings naturally arise [10,11]. An interplay of two different coupling ranges may lead to drastic effects in these systems; for instance, a global coupling can suppress turbulent dynamics generated by a local coupling, or it can select a given unstable mode of turbulence [12,13].

In this paper we study front instabilities in a two dimensional, forced oscillatory system, where interactions between the oscillators are realized by both local and global couplings. Our motivation for studying this system stems from the recent progress in controlling spatiotemporal chaos by a global feedback in experimental systems [14,15]. An interesting question is whether a similar control can be successfully applied for controlling front dynamics.

This work is organized as follows. In the following section we introduce our model: locally and globally coupled oscillators under external forcing. Section III is devoted to the linear stability analysis of the phase locked solutions. In Sec. IV, we show the pattern formation instability of the front. In Sec. V we study bifurcations of frontal patterns. In this section, the dynamics of a front line is studied numerically. Section VI is devoted to discussion.

II. THE MODEL SYSTEM

The model system under study is a globally coupled oscillatory system that is subjected to an external driving force whose frequency is twice that of the natural frequency of the oscillators. It can be described [7–9] mathematically as a parametrically forced complex Ginzburg-Landau equation (CGLE) for a complex scalar field $A(x,t)$,

$$\dot{A}=(1+i\omega)A+(1+i\alpha)\nabla^2 A-(1+i\beta)|A|^2A+\mu\overline{A}+\gamma A^*. \tag{1}$$

When $\mu=0$ and $\gamma=0$, Eq. (1) is the CGLE, a generic model for a system exhibiting a Hopf bifurcation at zero wave number and frequency ω_0. The last term in Eq. (1) represents the external forcing that breaks the phase symmetry of the system [16]. The frequency of the external forcing in Eq. (1) is twice of ω_0 [7]. The term $\overline{A}$ represents global coupling, i.e., a spatial average of A, $\overline{A}=C\int A dr$, where C is a normalization coefficient [10].

Obviously, the two last terms in Eq. (1) introduce more complex dynamics to the CGLE which is itself very rich [2]. However, we are concerned in this paper only with the front solutions of Eq. (1), which have analytic expressions in the variational, one-dimensional case for $\mu=0$. Indeed, when the real parameters α, ω, β, and μ vanish, Eq. (1) can be cast in a variational form

$$\frac{\partial A}{\partial t}=\frac{\delta F}{\delta A} \tag{2}$$

that admits solutions describing a front, or kink, which connects the two stationary solutions $A(x,t)=\pm A_0=\pm\sqrt{1+\gamma}$. There are two kinds of kink solutions, the first being an Ising wall

$$I(x;\sigma)=\sigma A_0 \tanh\left(\frac{1}{\sqrt{2}}A_0 x\right), \tag{3}$$

where $\sigma=\pm 1$ represents the polarity of the front. The other kind of solution is known as a Bloch wall

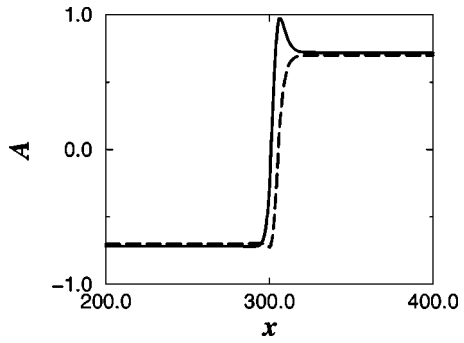

FIG. 1. A view of a nonvariational front. Solid line, ReA; dashed line, ImA. Parameters: $\omega=-0.825$, $\alpha=0.05$, $\beta=-1$, $\gamma=0.18$, $\mu=0$. All parameters, time, and space are dimensionless.

$$B(x;\sigma)=\sigma A_0\tanh(kx)+i\sigma\sqrt{1-3\gamma}\,\mathrm{sech}(kx), \qquad (4)$$

where $k=\sqrt{2\gamma}$.

It is known that the Ising wall is stable for $\gamma>\gamma_{cr}=\frac{1}{3}$, while the Bloch walls are stable for $\gamma<\gamma_{cr}$. Thus, γ_{cr} denotes the location of the front bifurcation in the limit of the vanishing α, β, ω, and μ [8].

Our objective in this paper is nonvariational analogues of these front solutions. As an example, in Fig. 1 we show a numerically obtained, nonvariational Bloch front in one dimension. Depending on the sign and intensity of global coupling, different perturbations to the front solutions can be expected. In this paper we focus on the spatial symmetry restoring effect of global coupling, which occurs for a small, negative μ. It strives for the spatial symmetry between the negative and positive amplitude domains. For example, in the absence of global coupling, the front in Fig. 1 propagates with a constant velocity, until it reaches a boundary. However, a front may change its direction of propagation under global coupling before reaching boundaries. This is shown in Fig. 2 as a gray scale space time plot. Figure 3 shows two snapshots of the front in Fig. 2, at the times of its propagation to the left and to the right.

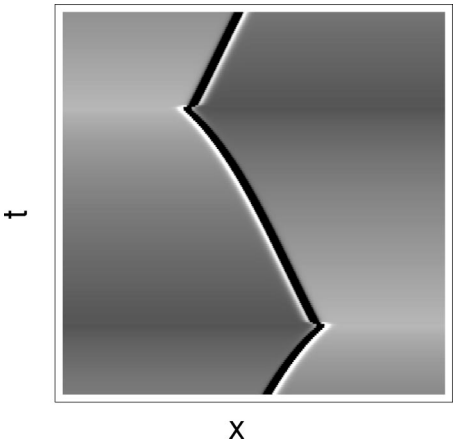

FIG. 2. Change of propagation direction under global coupling. $|A|$ is shown. The parameters are the same as in Fig. 1 except $\mu=-0.15$.

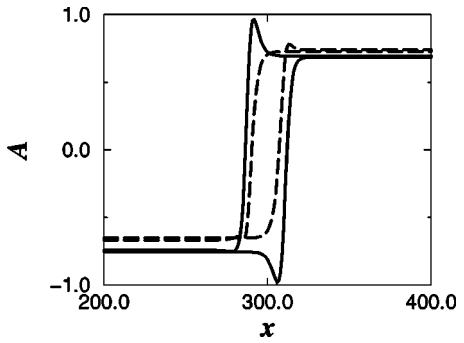

FIG. 3. Nonvariational fronts under global coupling. Solid line, ReA; dashed line, ImA. Two time moments are shown. The parameters are the same as in Fig. 2.

We found that the spatial symmetry restoring global coupling can stabilize in two dimension a circular domain that is unstable for $\mu=0$. The aim of this paper is to study front instabilities of this domain in the Benjamin-Feir unstable region where $1+\epsilon\beta<0$.

III. THE STABILITY OF THE PHASE LOCKED STATES

Nonvariational Ising and Bloch walls of Eq. (1) connect two spatially uniform phase locked states $A_{0n}=\pm(X_{0n}+iY_{0n})=\pm R\exp(i\phi)$, where R and ϕ are given by

$$\cos(2\phi)=(R^2-\tilde{\mu})/\gamma,$$

$$\sin(2\phi)=(\omega-\beta R^2)/\gamma,$$

$$R^2=\frac{\tilde{\mu}+\beta\omega+[\gamma^2(1+\beta^2)-(\omega-\beta\tilde{\mu})^2]^{1/2}}{1+\beta^2}, \qquad (5)$$

with $\tilde{\mu}=1+\mu$.

We study a linear stability of these phase locked states against the perturbations of the form $\delta A e^{iqx}e^{\lambda t}$. A linear stability analysis can be easily done, if the complex amplitude A in Eq. (1) is represented by the equations for its real X and imaginary parts Y [17]. The characteristic equation is given by

$$(\lambda-\tilde{\mu}-\gamma+q^2+A)(\lambda-\tilde{\mu}+\gamma+q^2+D)$$
$$=(-B-\omega+\epsilon q^2)(-C+\omega-\epsilon q^2). \qquad (6)$$

The A, B, C, and D in Eq. (6) are given by the following expressions:

$$A=3X_{0n}^2+Y_{0n}^2-2\beta X_{0n}Y_{0n},$$

$$B=2X_{0n}Y_{0n}-3\beta Y_{0n}^2-\beta X_{0n}^2,$$

$$C=3\beta X_{0n}^2+\beta Y_{0n}^2+2X_{0n}Y_{0n},$$

$$D=3Y_{0n}^2+2\beta X_{0n}Y_{0n}+X_{0n}^2. \qquad (7)$$

The relations, $A+D=4R^2$, $AD-BC=3(1+\beta^2)R^4$, and $B-C=-4\beta R^2$ allow elimination of X_{0n} and Y_{0n} from the characteristic equation. The root of Eq. (6), which leads to a pattern formation instability is

$$\lambda=\tilde{\mu}-2R^2-q^2+[1+\omega^2-(\omega-2\beta R^2-\alpha q^2)^2]^{1/2}. \quad (8)$$

In our previous paper we studied pattern formation of the phase locked states [17]. In this paper we are interested with the case when the phase locked states are stable, but the front is subject to pattern formation instability.

IV. PATTERN FORMATION OF THE FRONT

As analytical forms of front solutions are unknown in the nonvariational case, their linear stability analyses are not straightforward. Nevertheless, approximate analysis along a front position can be conducted to show pattern formation of the front.

Assume that in a two-dimensional system, two parallel, rectangular domains of equal size are chosen as an initial condition. Then, for the Ising front, $\bar{A}\to 0$. Assume also that the front is parallel to the y axis. By making a cross section perpendicular to the y axis, it can be seen (see Fig. 1) that a domain wall which connects the two phase locked states is an extended object along the x axis. By choosing an initial position in the x axis, a number of front lines parallel to the y axis can be drawn. These lines can be characterized by their amplitude values. For instance, the real part of their amplitudes are defined in the interval $0\leqslant|A_{front}(x)|<R$, where R is given by Eq. (5). As an Ising front is motionless and stable, a front line in this regime can be considered a steady, uniform state. In other words, in an Ising regime front lines behave like the phase locked states. Hence, a linear stability analysis of a front line can be conducted in the same way as it was done for the phase locked states [17]. If a number of these lines undergo a wave number instability, one can expect that the front exhibits the same instability. Therefore, we approximate the linear stability analysis of the front by the linear stability analyses of the front lines.

A linear stability analysis of the $A=0$ solution, i.e, the $A_{front}=0$ line, against perturbations $\delta A e^{iql}e^{\lambda_1 t}$ is given by

$$\lambda_1=\tilde{\mu}-q^2-\sqrt{\gamma^2-(\omega-\alpha q^2)^2}. \quad (9)$$

Note that l is a coordinate along the front line, which is parallel to the y axis. Along l, a linear stability analysis of the lines with $0<|A_{front}(x)|<R$ can also be performed. A perturbation of the $A=A_{front}(x)$ states by $\delta A e^{iql}e^{\lambda_2 t}$ leads to

$$\lambda_2=\tilde{\mu}-2|A_{front}(x)|^2-q^2+\{1+\omega^2 -[\omega-2\beta|A_{front}(x)|^2-\alpha q^2]^2\}^{1/2}. \quad (10)$$

In this paper, we will use γ as a control parameter. From now we fix other parameters at $\omega=-0.825$, $\alpha=2$, $\beta=-1$, $\mu=-0.15$. For these parameters and for $0.8\leqslant|A_{front}(x)|^2\leqslant 0.9$, Eq. (10) has linear spectra with a positive maximum at nonzero q. The two solid curves in Fig. 4 show linear spectra for the front lines $|A_{front}|^2=0.8$ and $|A_{front}|^2=0.9$.

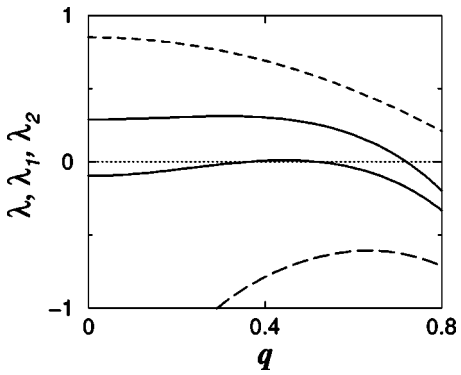

FIG. 4. Linear spectra for the fixed solution (long-dashed line), for front lines with maximum unstable modes (solid lines), and for $A=0$ solution (dashed line). $\gamma=0.38$.

These curves display positive maxima at some critical q_{cr}. The dashed curve in Fig. 4 shows linear spectra for the $A_{front}=0$. It has a positive maximum at $q=0$. There is no positive maximum for the phase locked states $R^2=1.17$ (long-dashed curve); all wave numbers are stable for this case. Thus, Fig. 4 shows that for parameters we have chosen, several front lines have the most unstable mode; hence, under suitable conditions leading to a wave number selection, pattern formation can be expected in the neighborhood of these lines.

In our simulations with $\mu=0$, a narrow parameter region was detected for a clearly pronounced, stable pattern formation of the front. Moreover, with the change of the control parameter, a front transition leading to a collapse of domain may occur.

Numerical results show that for a small and negative value of μ, the phase locked solutions, as well as the nonvariational domain walls, still remain structurally stable. But more importantly, regardless of their initial sizes two domains acquire an equal size if $\mu<0$. This means that if an initial condition is chosen to be two domains, then at a sufficiently long run, $\bar{A}\to 0$. Unlike the case $\mu=0$, there is no collapse of a domain. With a gradual decrease of γ, global coupling continues to force $\bar{A}\to 0$, and this delays the front transition. Thus, the front remains almost stationary for an interval of the control parameter. Before the onset of an Ising-Bloch transition, pattern formation can be detected. This is shown in a three-dimensional plot of a front in Fig. 5. There are no pattern formations for the phase locked solutions in Fig. 5, but the front exhibits roll patterns. The wavelength of the roll patterns is given by

$$q_{cr}=\left[\frac{1+\omega\alpha}{1+\alpha^2}-2|A_{front}|^2\frac{1+\alpha\beta}{1+\alpha^2}\right]^{1/2}. \quad (11)$$

A Fourier transform of the roll patterns in Fig. 5 shows that from the spectrum of the critical wave numbers displayed by the front lines, a wave number for the line with $|A_{front}|^2\approx 0.9$, which has a larger critical wave number has been selected. Note that the selected pattern covers all front areas in Fig. 5, though according to the linear stability analysis near the region corresponding to $A=0$, no pattern formation

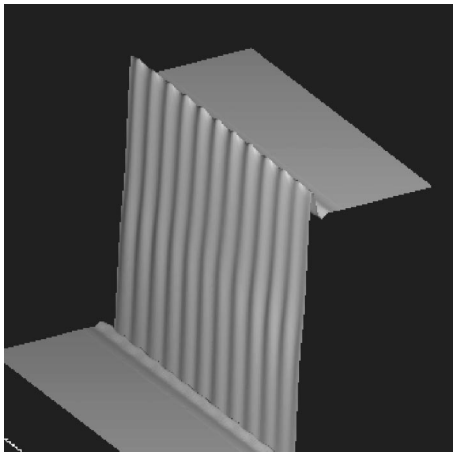

FIG. 5. A three-dimensional view of ReA. $\gamma=0.38$.

was expected. However, it can be shown that for a slightly larger value of γ, pattern formation emerges only at certain areas of the front, in accordance with the linear stability analysis.

V. FRONT LINE INSTABILITIES

In this section we numerically study Eq. (1) in dimension two. The numerical method is described in Ref. [17]. The system size is $L_x=L_y=256$, $\delta x=0.5$, $\delta t=0.02$. As an initial condition, we take a small rectangular domain inside a larger rectangular domain. If $\mu=0$, the larger domain would invade the smaller one; however, the presence of a global coupling term forces $\overline{A}\to 0$, and it stabilizes a circular domain. A front is an interface between the domains. In Fig. 6, it is the area between the darkest and brightest circles. The core of the front can be defined as the region where the real amplitude $|A|$ approaches its minimum. In an Ising regime, a front has a regular shape. With the decrease of γ, the front losses its circular shape, but a cellular pattern along the front emerges, as in Fig. 6(b). This pattern formation is associated

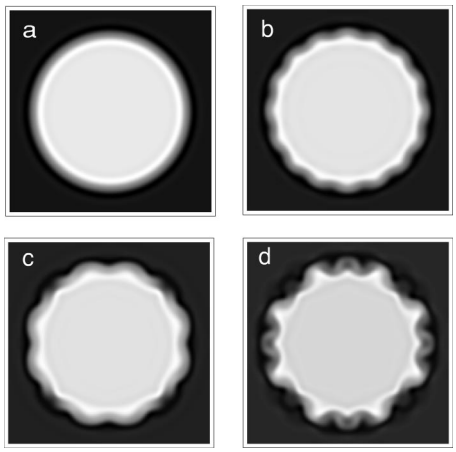

FIG. 6. Front dynamics versus γ. ReA is shown. (a) Ising regime; $\gamma=0.4$. (b) Pattern formation along the front line; $\gamma=0.38$. (c) Wave trains; $\gamma=0.37$. (d) A weak turbulence of wave trains; $\gamma=0.32$.

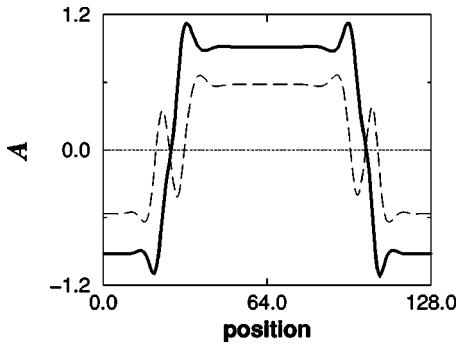

FIG. 7. A typical view of a nonvariational Ising wall. The solid line shows the imaginary part, and the dashed line shows the real part of the complex amplitude A. $\gamma=0.4$.

with the most unstable wave number of the front lines, as discussed in the preceding section.

With the further decrease of γ, the pattern along the front starts to propagate, Fig. 6(c). For the set of parameters used in Fig. 6, $\lambda<0$ for all q in Eq. (10) (see the long-dashed curve in Fig. 1). Hence, the phase locked solutions are stable, and the inner part of the domains are uniform. Therefore, the pattern propagation along the front gives the impression of a domain rotation. Further decrease of γ causes chaotic patterns along the front, as in Fig. 6(d). Thus, Figs. 6(b)–6(d) illustrate that front instabilities precede an Ising-Bloch transition. We note that at $\gamma_{cr}\approx 0.25$, an Ising-Bloch transition occurs, and the white domain in Fig. 6 starts to travel through the dark domain. In this regime, very complicated structures can be seen along the front of a moving domain.

A typical amplitude profile in an Ising regime is shown in Fig. 7. As structure of Re(A) is rather simple then ImA, we will use the real part ReA for a characterization of a front line location and its dynamics. For simplicity, we define a variable which is given by distance from the center of the system (x_0,y_0) to the front line where $A=0$, $r=\sqrt{(x_0-x_{\mathrm{Re}A=0})^2+(y_0-y_{\mathrm{Re}A=0})^2}$. To plot this variable we choose a position on the front line and calculate r for it. Then, moving clockwise, we search for the next closest point where $\mathrm{Re}|A|=\mathrm{Re}|A_{min}|$, and r for this point is calculated. In this way, we calculate and record r's value along the front until the first point is reached and the front line is closed. For instance, if a front line has a circular shape, as in Fig. 6(a), $r=$ const. Thus, plotting of r will produce a line. For a front like that shown in Fig. 6(b), the plotting of r will produce a regular periodic structure.

In Fig. 8, we show a gray-scale space time plot of r for three different values of γ. Note that to save space we have shown dynamics only on the quarter part of the front line. The first column in Fig. 8 shows Turing-Hopf-like structures, one-dimensional cellular structures that appear in an oscillating manner. With the decrease of γ, cellular structures start to propagate with a constant velocity, as shown in the second column of Fig. 8. In this regime, global coupling still remains small, but its oscillation near zero causes perturbations which trigger wave trains. With the further decrease of γ, a partial deformation of cellular structures occurs, and it seems that the emerging dynamics can be best characterized as a

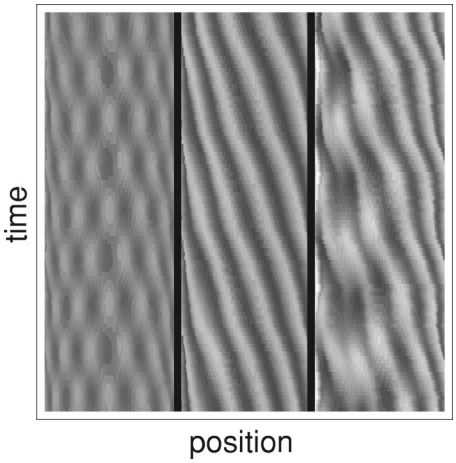

FIG. 8. Space time plots of structures formed by a front line. From the left, the Turing-Hoph pattern, traveling waves, and front turbulence.

weak turbulence of wave trains [6], as seen in the last column of Fig. 8.

In Fig. 9 we over plot the front line $A_{front}=0$ at three different time moments when the system is in a regime corresponding to the last column of Fig. 8. The values of r along the front line at a given moment are shown in Fig. 10. We calculated temporal and spatial correlation functions of $\Delta r(l,t)=r(l,t)-\overline{r}(t)$, where $\overline{r}$ is the spatial average of r. These functions are defined by

$$C_{\Delta r}(t)=\langle \Delta r(l',t)\Delta r(l',t+t')\rangle/\langle(\Delta r)^2\rangle,$$

$$C_{\Delta r}(l)=\langle \Delta r(l,t')\Delta r(l+l',t')\rangle/\langle(\Delta r)^2\rangle, \tag{12}$$

where $\langle\cdots\rangle$ represents an average over l' and t'. In Fig. 11 we show $C_{\Delta r}(t)$ for two different γ. As the solid line in Fig. 11 shows, at smaller t, $r(l)$ oscillates around its mean almost periodically. However, as t grows these oscillations become irregular. With the decrease of γ, correlation time slightly increases, the dashed line Fig. 11. It means that the frequency of r's oscillation near its mean decreases with the decrease of γ. Figure 12 shows spatial correlation functions at two different γ. The decay of $C_{\Delta r}(l)$ is not sharp at small x; longer waves are dominant in the spatial distributions of r. Correlation length also increases with the decrease of γ, Fig. 12 the dashed line. Numerical experiments show that the front width increases with the decrease of γ. Such increase in width weakens small scale spatial perturbations to r. Slow decays of temporal and spatial correlation functions in Figs. 11, 12 indicate a weakness of turbulent dynamics.

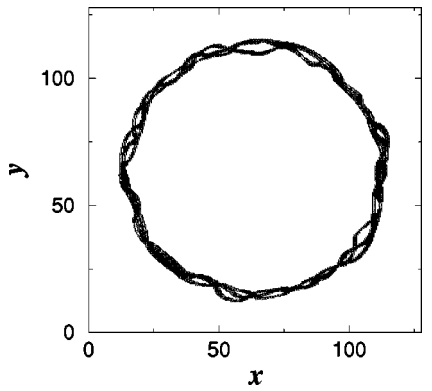

FIG. 9. Overplots of a front line exhibiting turbulence. Three different time moments are shown.

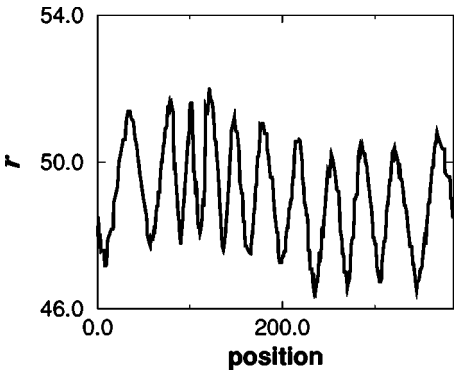

FIG. 10. A chaotic pattern along the front line.

In Fig. 13, we plot a long time average $\langle\Psi_q^2\rangle$ versus q, where $\Psi_q=\int r(l)\ e^{iql}\ dl$. A high spectrum at small q is due to the perturbations of global coupling. The maximum at $q\neq 0$ corresponds to $q\approx 0.4$ which is close to the q_{cr} given by Eq. (11). Shorter waves in Fig. 13 decay by a power law, $\langle\Psi_q^2\rangle\sim q^{-\sigma}$, with $\sigma\approx 2.45$. With the decrease of γ, the maximum gradually disappears and σ decreases. Interestingly, having a maximum and a power law decay at shorter waves are known features of the fluctuation spectrum of a stationary turbulent state of the KS equation. However, in the phase turbulence of the KS, shorter waves decay by $\langle\Psi_q^2\rangle\sim q^{-\sigma}$, with $\sigma=2$. This implies loss of long range order [6]. For parameters we have fixed, the fluctuation of $[\partial r(l)/\partial l]$ seems to depend on q. Thus, unlike the phase turbulence in the KS, a coherence loss might be slower in our case. More accurate computations are desirable in different parameter regions of Eq. (1), and for larger system size to elucidate scaling nature of the front line turbulence.

VI. DISCUSSION

Pattern formation and turbulence of a wave front in general, two-dimensional reaction diffusion models with bistable

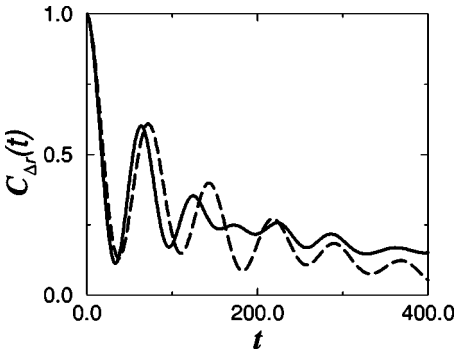

FIG. 11. Time correlation functions. Solid line, $\gamma=0.32$; dashed line, $\gamma=0.28$.

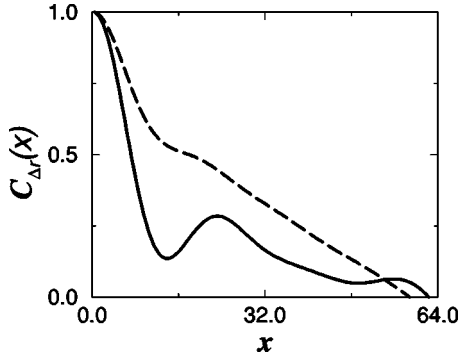

FIG. 12. Spatial correlation functions. Solid line, $\gamma = 0.32$; dashed line, $\gamma = 0.28$.

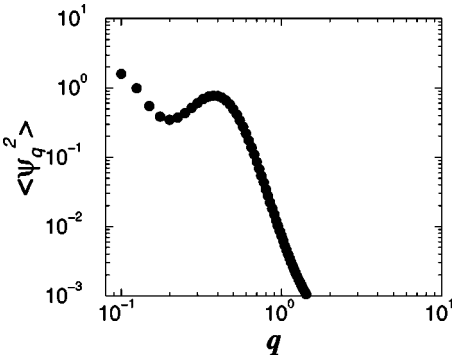

FIG. 13. Log-log plot of fluctuation spectrum of chaotic patterns formed by the front line.

kinetics were theoretically predicted a few decades ago [5,6]. Later, these front instabilities have been studied in a reaction diffusion system with autocatalytic kinetics [18,19]. Recently, complex front dynamics have been studied in a two-dimensional oscillatory medium in the 3:1 resonance regime, i.e., when the external forcing frequency is three times of the natural frequency [20,21]. We have shown in this paper pattern formation and a weak turbulence of the front in the 2:1 resonance system with a global coupling. We studied front dynamics of a circular domain which is unstable in the absence of global coupling. However, for special initial and boundary conditions [20], global coupling is not necessary for stabilization of a band shaped domain. A front of such domain shows the effects we have discussed here. We found that the spatial symmetry restoring perturbations significantly widens a parameter region for these effects.

Our simulations show that global coupling can change direction of front propagation in the 2:1 resonance system. However, we found that the spatial symmetry restoring global coupling does not control the width of front. Besides, as a result of alternation of propagation direction, correlation time, and length of the function Δr which characterizes front line location may drop significantly. Thus, global coupling can be a destabilizing factor for the front line position.

Finally, we suppose that the front line instabilities we have studied in this paper can be observed in experimental systems.

ACKNOWLEDGMENT

The author thanks Professor A. S. Mikhailov for discussions.

[1] A. S. Mikhailov, *Foundations of Synergetics I. Distributed Active Systems*, 2nd revised ed. (Springer-Verlag, Berlin, 1994).
[2] M. C. Cross and P. C. Hohenberg, Rev. Mod. Phys. **65**, 851 (1993).
[3] G. Haas, M. Bar, I. G. Kevrekidis, P. B. Rasmussen, H.-H. Rotermund, and G. Ertl, Phys. Rev. Lett. **75**, 3560 (1995).
[4] T. Frisch, S. Rica, P. Coullet, and J. M. Gilli, Phys. Rev. Lett. **72**, 1471 (1994).
[5] Y. Kuramoto, Prog. Theor. Phys. **63**, 1885 (1980).
[6] Y. Kuramoto, *Chemical Oscillations, Waves, and Turbulence* (Springer-Verlag, Berlin, 1984).
[7] P. Coullet, J. Lega, B. Houchmanzadeh, and J. Lajzerowicz, Phys. Rev. Lett. **65**, 1352 (1990).
[8] C. Elphick, A. Hagberg, B. A. Malomed, and E. Meron, Phys. Lett. A **320**, 459 (1997).
[9] P. Coullet and K. Emilsson, Physica D **61**, 119 (1992).
[10] G. Veser, F. Mertens, A. S. Mikhailov, and R. Imbihl, Phys. Rev. Lett. **71**, 935 (1993).
[11] K. C. Rose, D. Battogtokh, A. Mikhailov, R. Imbihl, W. Engel, and A. M. Bradshaw, Phys. Rev. Lett. **76**, 3582 (1996).
[12] D. Battogtokh and A. S. Mikhailov, Physica D **76**, 84 (1996).
[13] D. Battogtokh, A. Preusser, and A. S. Mikhailov, Physica D **106**, 327 (1997).
[14] C. Day, Phys. Today **54**(7), 18 (2001).
[15] M. Kim *et al.*, Science **292**, 1357 (2001).
[16] C. Elphick, G. Iooss, and E. Tirapegui, Phys. Lett. A **120**, 459 (1987).
[17] D. Battogtokh and D. Browne, Phys. Lett. A **266**, 359 (2000).
[18] S. K. Scott and K. Showalter, J. Phys. Chem. **96**, 8702 (1992).
[19] D. Horvth, V. Petrov, S. K. Scott, and K. Showalter, J. Chem. Phys. **98**, 6332 (1993).
[20] C. Hemming and R. Kapral, Faraday Discuss. **120**, 371 (2001).
[21] R. Kapral, R. Livi, and A. Politi, Phys. Rev. Lett. **79**, 2277 (1997).